LM-06K041
April 24, 2006

Phase Transitions Involving Dissociated States of Water at the Electrochemical Ni(111)/H_2O Interface

C Taylor, R Kelly and M Neurock

Phase transitions involving dissociated states of water at the electrochemical Ni(111)/H_2O interface

Christopher Taylor[1], *Robert G. Kelly*[1], *Matthew Neurock*[2]

[1]Department of Materials Science and Engineering

[2]Department of Chemical Engineering

University of Virginia

Charlottesville, VA 22904-4745

Electrochemical processes occurring in aqueous solutions are critically dependent upon the interaction between the metal electrode and the solvent. In this work we use density functional theory to calculate the range of potentials for which molecular water and its activation products (adsorbed hydrogen and hydroxide) are stable when in contact with an immersed Ni(111) electrode. Changes in the adsorption geometries of water and its dissociation products are also determined as functions of potential. We find that, at zero Kelvin, interfacial water activates to form a hydroxide overlayer at potentials anodic of -0.5 V NHE. The cathodic activation of water to form a surface hydride occurs at potentials cathodic of -0.3 V NHE. There is therefore a potential range at which both H and OH form on the surface, in agreement with inferences made from the experimental literature. The surface hydroxide/oxide transition occurs at 0.2 V NHE. The increased binding of oxygen to the surface at progressively anodic potentials correlates with weakening nickel-nickel interactions and the lifting of a metal atom above the surface plane. Thermodynamic extrapolations are made to ambient (300 K) and elevated (600 K) conditions and Pourbaix-type diagrams are presented for the inert and activated surface phases of water on Ni(111).

1. Introduction

The electrochemical behavior of water on metal surfaces is of profound theoretical and practical importance. Interfacial water assists many catalytic and electrocatalytic processes; leads to the activation of the metal and the formation of passive oxides or hydroxides on metals such as nickel, aluminum and zinc; actively participates in the deleterious processes of leaching, corrosion, and environmentally assisted cracking; and provides the interface for biological adhesion to metal substrates. An understanding of the atomic structure of water at the electrochemical interface is therefore critical to the rational design of electrocatalysts, corrosion resistant alloys, and biomimetic scaffolds between biological substrates and metal surfaces. Whereas experimental techniques, such as surface enhanced Raman spectroscopy, *in situ* electron microscopy and crystal rod truncation techniques are now beginning to capture some of the chemical changes occurring at the electrochemical interface[1, 2], there is still a significant demand for theoretical insight. The recently developed abilities to directly observe potential-dependent interfacial phenomena such as changes in molecular structure[3, 4], chemisorption[5, 6], water activation[7] and surface reconstruction[8] require the development of competitive theoretical models that can incorporate electrochemical surface phenomena into an overall predictive and interpretive framework.

The complex structure of the interface between an electrode and solution and its dependence upon the electrochemical potential has stimulated theoretical debate for over one hundred years[9]. As physical descriptions of ionic motion, solid-state electronic structure, and water dynamics have evolved, so too have models of the electrochemical interface. The recent model of Sidik and Anderson captures this progression[10, 11], by

adopting a complex quantum model of the reaction center, with a local solvation shell, embedded in a Madelung psuedo-crystal environment that simulates the electrolyte.

A key difficulty in modeling electrochemical processes has been the inclusion of a reference electrode within the simulation via which the electrochemical potential can be established. Anderson and co-workers addressed this difficulty by equating the ionization potential / electron affinity for the reaction center to be oxidized/reduced with the absolute potential with reference to the free (vacuum) electron. Potentials relative to the hydrogen electrode may then be determined using Trasatti's equation[12]:

$$V_{NHE} = V_{abs} - (4.6 \pm 0.2)\ V \qquad [1]$$

In the absence of a sufficient model for the surrounding solvent and counter-charge, however, electrochemical potentials derived using reaction-core cluster models for the electrochemical interface are weak approximations. Such systems can not be readily tuned for varying surface charge densities/applied electrochemical potentials, except by the location of distant ions with known ionization potentials/electron affinities (an approach also adopted by Crispin *et al.*[13]). However, the meticulous creation of detailed reaction site models with fine control over the reaction coordinate has allowed significant insight into the interplay between electronic and structural effects occurring during redox processes upon electrode surfaces.

Other models of the interface have involved the use of tight binding methods, or image potentials, which are successful at capturing phenomena at modest distances from the electrode, such as localized ordering of water within 5 Å of the electrode, and important effects such as ion diffusivity and local residence times. The ability to model phenomena on these size scales, however, comes with a loss of chemical resolution, because such

models are unable to capture bond-breaking and bond-creation processes. Furthermore, the behavior of water at the electrochemical interface is controlled by the fine balance between interactions with the solvent and adsorption processes at the electrode. Such tensions hinge upon the balance of small energic effects (typically fractions of an eV)[14] which can only be probed reliably using full quantum mechanical methods.

The tremendous advances in processing power, along with the advances in theoretical methods that have occurred over the past decade, however, has allowed us the ability to simulate systems comprised of hundreds of atoms covering nanometer size scales via first-principles methods. Interfacial models developed at these size scales are sufficient to capture the shape of the electrostatic potential across the interface and, consequently, to establish a model reference electrode within the system. Such a model, involving two reference 'electrodes', was proposed by Filhol and Neurock in their model of water activation by Pd(111)[15]. The first reference establishes the absolute potential, which is derived from a first-principles calculation of the spatial distribution of the electrostatic potential of a neutral model of the reaction center in contact with a 10-20 Å vacuum region. The potential of polarized states is then measured with reference to an internal solution phase 'electrode' placed at an optimum distance from the electrode face. By performing first principles calculations in a periodic slab ensemble, Filhol's method successfully captured the bond-making and bond-breaking processes occurring during the electrolytic activation of water over Pd(111). Polarization of the interface was achieved by charging the metal electrode with a pre-determined number of electrons, while a homogeneous counter-charge maintained neutrality. In reality, charge neutrality is maintained by the localized presence of counter-ions, as described in the Gouy-Chapman

diffuse electrolyte model[16, 17]. Calculations by Taylor et al. have demonstrated the ability for homogeneous counter-charge methods to effectively mimic the electric field at the solution/electrolyte interface[18].

In this work we apply the double-reference method to the activation of water by polarization of a Ni(111) surface. Nickel-based alloys are commonly employed in engineering applications due to their high strength and high corrosion resistance. Even in high-purity water, however, corrosion of such alloys can occur, particularly via stress corrosion cracking (SCC). Two primary SCC mechanisms have been proposed: embrittlement occurring due to hydrogen uptake at the crack tip, and atomic dissolution of the metal at the exposed surface. Current opinion regarding these two mechanisms is inconclusive, largely due to the inability to directly observe processes occurring at the crack tip.

Performance tests of nickel alloys in high-purity water by Young et al. revealed that up to order of magnitude increases in crack-growth rate occur when conditions at the metal surface activate the Ni/NiO transition[19]. These results suggest that a unique surface environment exists at the equilibrium potential for this transition. Suzuki and coworkers[20] studied phase transitions on the single-crystal Ni(111) surface plane in contact with a Na_2SO_4/H_2SO_4 solution at pH 3 using scanning tunneling microscopy (STM) and found that the surface was bare and unreconstructed up to -0.16 V NHE. Above this potential nickel began to dissolve at step edges on the surface. At +0.09 V a surface film starts to form. While Suzuki et al. attributed this film to oxide formation, the in situ infrared spectroscopy and STM observations by Nakamura et al.[21] imply that the overlayer consists of hydroxyl species and ultimately $Ni(OH)_2$. Substantial surface

reconstruction was observed as the activated nickel surface adopted the configuration of $Ni(OH)_2$. The equilibrium potential at pH 3 for hydroxide formation reported by Nakamura et al. was 0 V NHE. Experimental studies of crack tip chemistry and electrochemistry in high temperature, high purity water are of extreme difficulty. Thus, fundamental understanding of the processes occurring is sorely limited.

Similar studies by the Marcus group on copper and silver surfaces, revealed the progressive formation of hydroxyl overlayers, followed by the creation of a bulk oxide, that initiates at step edges.[5, 22-25] In a previous study we simulated the oxidation of water on Cu(111) and have shown that oxide formation is synchronous with destabilization of the electrode surface[26]. Both this paper, and the paper by Filhol[15], are limited in their application to experimental conditions, however, due to the creation of protonated water molecules (and thereby unrealistic pH environments) within the nanometer dimensioned unit cell. Herein we develop Filhol's original methodology to allow the diffusion of interacting species to and from the model system via the inclusion of energetic terms for the chemical potential of such species. Proton diffusion and the extrapolations of energetic data obtained at zero Kelvin make it possible to model the thermodynamics at arbitrary pH and temperature.

2. Computational Details

The Ni(111)-H_2O interface was modeled using the periodic gradient-corrected plane-wave density functional theory as implemented in the Vienna Ab initio Simulation Package developed by Kresse and Hafner[27-29]. The metal/water interface was examined using a periodic slab architecture in which the electrode is defined by three or five layers

of metal atoms and the solution phase placed between the metal slab with a density equal to that of liquid water at 298 K (1.0 g/cm^3). The coordinates of metal atoms in the center layer are held fixed at the experimentally determined bulk Ni-Ni distance. Water molecules were arranged following the bilayer model of Doering and Madey, with the exception that only a half-bilayer is present immediately adjacent to the electrode, following the results of recent molecular dynamics simulations that indicate a reduced density of liquid water molecules at the surface compared to that occurring during UHV (ultra-high vacuum) deposition. The dimensions of the supercell were $a = b = 7.475$ Å, $c = 22.41$ Å; $\alpha = \beta = 90^o$, $\gamma = 120^o$. A super-cell was constructed containing 27 Ni atoms for the three-layer model of the electrode (three layers of p(3x3) Ni(111); 36 Ni atoms were used for the five-layer model) and 24 water molecules (3 bilayers + 2 half-bilayers). One such supercell is shown in Figure 1.

Ionic and core interactions were modeled via relativistic PW91 Vanderbilt ultra-soft pseudopotentials[30] provided by Kresse and Hafner[31], and an energy cut-offs of 396 eV was used for the plane-wave basis set. Calculations were performed using the RPBE exchange-correlation functional[32, 33] and a 3x3x1 Monkhorst-Pack k-point mesh[34]. Self-consistent electronic structure calculations were converged to 0.1 meV and atomic structures were converged to 1 meV.

The electrochemical potential was varied by increasing or decreasing the total electron density available to the model systems. To maintain neutrality in the periodic ensemble, a homogenous background charge distribution of the appropriate density, ρ, was introduced across the entire cell volume. To compare energies between a charged and uncharged system, the energy of the added (or subtracted) electrons and the energy of the

countercharge were subtracted from the total energy. The correction term is calculated from the absolute potential of the system, V_{abs}, and the average electrostatic potential of the unit cell, $<\phi>$, as follows:

$$E_{corr} = V_{abs}.q_e + \int <\phi> \rho \, d\Omega \qquad [2]$$

The integration is performed over the entire volume of the unit cell, Ω. The absolute electrochemical potential was determined via the creation of a secondary slab system having a 15 Å void inserted in the centre of the water layer. The electrostatic potential over this region corresponds to the potential of the free electron, which serves as a reference point to the total system Fermi potential. Potentials may then be referenced to the normal hydrogen electrode using the formula:

$$V_{NHE} = V_{abs} - V^{r}_{NHE}(T) \qquad [3]$$

$V^{r}_{NHE}(T)$ is the absolute half-cell potential of the H_2/H^+ couple calculated at the same level of theory used in this work and using thermodynamic expressions to extrapolate the potential to ambient and elevated temperatures, using the following thermodynamic cycle in like manner to Llanos and Errickson:[35]

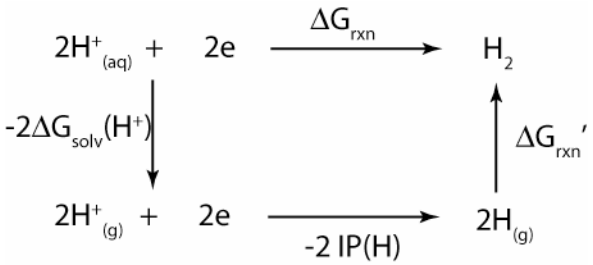

Scheme I

The entropic terms for H_2 arise from the translational and vibrational degrees of freedom calculated at the RPBE level of theory. The absolute potential of the H_2/H^+ electrode is defined as the potential required to set ΔG_{rxn} to 0 (*i.e.*, the equilibrium

potential). Using the cycle in Scheme 1 we calculate V_{abs}^{NHE} to be 4.51, 4.67 and 5.63 at 0 K, 300 K and 600 K respectively.

Absolute potentials of non-neutral systems cannot be reliably calculated via the vacuum reference method due to interference from the background charge, and are instead calculated with reference to an aqueous reference electrode that is maintained between both neutral and polarized systems. Further information regarding this method can be found in the paper by Taylor et al.[18]

Frequencies of atomic vibration were calculated for the adsorption phases of H, H_2O, OH and O using the harmonic approximation by varying the coordinates of the adsorbed atoms. The corresponding zero point vibrational energies and temperature extrapolations were made using standard statistical mechanics.

When water is electrochemically activated to form a surface hydride or hydroxide, a proton is either created or consumed. To simulate processes occurring in dynamic liquid environments, we consider the proton to diffuse to or from a solution-phase region outside the simulation cell. By thus excluding the proton from our model interface we are able to maintain a neutral pH within the simulation. The chemical potential of the proton was then included in the thermodynamic calculations by referencing to the pH, ionization potential and solvation energy of the aqueous proton as determined from the literature[36-39].

3. Results and Discussion

Reconstruction and thermodynamic response to surface polarization at 0 K

The optimized structure of the Ni(111)/water interface is presented in Figure 1. A range of potentials between -2 and +0.5 V NHE was considered by adding or subtracting between 0.0 and 1.0 electrons per unit cell. The interfacial capacitance, *dq/dV*, so derived is 9.0 μF/cm^2. The potential of the neutral slab is 0.07 V NHE, close to the experimental potential of zero charge (-0.02 V). As noted in the Methods section, the electrochemical potential calculated using Filhol's method is the average potential difference across the two unique interfaces of the periodic slab (note the difference between the orientations of the upper and lower water layers with respect to the periodic metal slab in Figure 1). By studying the orientation of water at either side of the periodic Ni(111) slab, we deduce that the potential so calculated is an average between the interfacial potentials for a nickel electrode saturated with positively oriented water dipoles, and a nickel electrode saturated with negatively oriented dipoles. It is anticipated that this will therefore roughly correlate to the potential of a interface with dynamically fluctuating water dipole orientations, assuming that the thermal energy of the liquid is on the same order as the competition between metal-water interactions and water-water interactions. Theoretical calculations by Michaelides et al.[40] showed that the metal-water bond is significantly weaker than a hydrogen-bond, a result which was also supported by the surface studies of Nakamura et al.[41].

In Figure 2 we present the variation in structural parameters of interfacial water as a function of electrochemical potential. Parameters are reported for water at the lower interface. Squares denote the inclination of the water dipole above the plane parallel to the surface, and circles denote the height of the water oxygen atom above the surface plane of nickel atoms. At cathodic potentials, towards the hydrogen evolution potential,

the water dipole is oriented 15^{o} above the horizontal. As the potential is made increasingly anodic, the water dipole at the lower interface rotates away from the positively charged surface and the Ni-O interaction becomes stronger. The Ni-O bond length decreases by 0.2 Å over the potential range -2 to +0.5 V NHE and the water dipole rotates through an angle of 20^{o}. The geometry at the upper surface does not change noticeably as a function of potential. We suggest that this is due to the substantially diminished interaction between the hydrogen atoms of water with the nickel substrate compared to nickel-oxygen interactions occurring at the lower surface.

We have applied the same polarizations to a five layer Ni(111) model electrode in contact with the water network. The variations both in structure and potential for the five-layer slab coincide with those observed for the three-layer slab (see Figure 2, open symbols), indicating that the three-layer slab is sufficient to model surface effects.

Sebastiani and Delle Site[42] calculated Ni-O bond lengths of 2.26 Å for water at the atop site on the terrace of an unpolarized Ni(211) surface. This value is in agreement with the value determined in our work at the potential of zero charge. To our knowledge, nobody has hitherto explored the potential-dependent structure of the Ni/H_2O interface. Qualitative features, such as the re-orientation of water dipoles upon cathodic and anodic charges, and the repulsion of H_2O from the interface at cathodic potentials, have been observed in semi-classical molecular dynamics simulations on Cu(110) by Halley and Price[43].

The optimized structure for water on Ni(111) bears resemblance to the bilayer structure of water at a metal surface proposed by Doering and Madey[44], and that the bilayers propagate throughout the water matrix in like fashion to the crystal structure of ice Ih[45].

The structure differs from an exact bilayer, however, by the formation of only a half-bilayer immediately adjacent to the electrode. A more comprehensive mapping of the surface morphology of interfacial water, including comparison to 'whole bilayer' interfaces, was not pursued in this work. Additionally, we find that absolute proton ordering is obeyed in our model system, giving rise to ferroelectric effects. Whereas ferroelectric ordering is not observed even in low temperature ice samples[44], local hydrogen bonding dictates certain hydrogen bond patterns at the low-temperature interface. The reader should be aware that this structure is only one of many possible at the interface between water and the nickel electrode. We have assumed in this work that interfacial phenomena such as adsorption can be modeled independently of the structural perturbation of water far from the interface.

Next we considered the electrochemical activation of water on Ni(111). Water may be reduced to form a surface hydride and a solvated hydroxide moiety (4), or oxidized to produce surface hydroxyl and a solvated proton (5):

$$Ni(111)\text{-}H_2O/H_2O \rightarrow Ni(111)\text{-}H/H_2O + OH^-\ (aq) \qquad [4]$$

$$Ni(111)\text{-}H_2O/H_2O \rightarrow Ni(111)\text{-}OH/H_2O + H^+\ (aq) \qquad [5]$$

The adsorbed hydroxyl species can be subsequently oxidized to produce an oxygen adatom and another released proton (6):

$$Ni(111)\text{-}OH/H_2O \rightarrow Ni(111)\text{-}O/H_2O + H^+\ (aq) \qquad [6]$$

Having previously considered the structure and potentiostatic response of water on Ni(111), we now examine in the following sections the electrochemical behavior of adsorbed hydrogen, hydroxyl and oxygen on the Ni(111) surface.

To investigate the potential-dependent thermodynamics and structure of hydrogen on Ni(111), we created a model system with hydrogen adsorbed on a nickel electrode in an aqueous environment. Studies on clean Ni(111) surfaces and surfaces with water bilayers show that hydrogen preferentially adsorbs at the hcp three-fold hollow (the fcc site is only marginally less stable, +0.01 eV)[46-49]. We place the hydrogen atom at an hcp site on the Ni(111) surface as shown in Figure 3. The hydrogen atom is placed at the positively oriented end of the water matrix since this particular orientation of water suggests its preferential activity for reductive processes such as hydrogen uptake and evolution.

The height of hydrogen above the surface at different potentials is shown in Figure 4. We see that hydrogen at the hcp site is repelled at anodic potentials, and attracted towards the electrode at cathodic potentials. This result is consistent with the reductive chemistry of hydrogen on nickel as well as other electrodes. The effect is not large, however. The distance changes from 0.94 to 0.96 Å over a potential range of 4 V.

Adsorption of atomic hydrogen on the neutral slab changes the electrochemical potential to 0.24 V NHE. The capacitance of the system also drops substantially (from 9.0 $\mu F/cm^2$ to 4.8 $\mu F/cm^2$) indicating that interaction of hydrogen with surface states on Ni(111) reduces the capacity of the interface to store charge. The adsorption of hydrogen therefore requires a non-Faradaic transfer of electric current to the electrode to maintain constant potential. We have calculated the change in surface charge density as the product of the interfacial capacitance and the potential difference (0.8 $\mu C/cm^2$).

We next considered the state where water is deprotonated to produce a hydroxyl overlayer on the surface (Figure 5). The excess proton was not included in the unit cell as the diffusion event was assumed to be rapid, and therefore to have occurred prior to

reaching equilibrium at the interface. We thereby were able to maintain the (uncalculable[50]) pH environment within the < 1 $(nm)^3$ unit cell. The optimum geometry for the system with OH adsorbed at the hcp site is illustrated in Figure 5. The geometric and energetic response of the system to an applied potential over the -2 through +2 V NHE range was calculated. It was found, like hydrogen, that the geometry of the hydroxyl overlayer does not vary markedly as a function of potential, as shown by the small change in optimal Ni-OH distance with potential (Figure 6). Patrito and Paredes-Olivera[51], as well as Koper and van Santen[52], found that the geometry of OH on Ag(111) changes only marginally when an electric field is applied.

The potential of zero charge, calculated to be 0.04 V, and the capacitance of 9.3 $\mu F/cm^2$ differ little from the parameters calculated for the inert water phase. We attribute this similarity to the coincidence between the net dipole orientation and electron transfer effects of the OH and H_2O adsorbates.

A second dissociation step leads to the formation of adsorbed atomic oxygen at the Ni(111)/H_2O interface. Again we consider the formation of a low coverage monolayer as shown in Figure 7. Like hydroxyl and hydrogen, the oxygen is preferentially bound at the hcp hollow site, although previous calculations on both Cu(111) and Ni(111) show only small differences in the stabilization energy for hcp and fcc binding sites (<50 meV)[26, 53]. As the potential is varied we observe not only changes in the adsorbate geometry, but also an effect upon the Ni(111) substrate. In Figure 8 we present the changes in the Ni-O bond length (measured as the distance of O from the surface plane) and changes in the Ni-Ni bond length (measured similarly as the height of the adatom above the surface (111) plane). The Ni adatom lifts out of the surface as the potential becomes more

anodic. This can be partially observed in the neutral system shown in Figure 7. Over the potential range from -2 to +1 V NHE the Ni(111)-Ni* distance increases from 0.29 to 0.72 Å. Such steps towards dissolution and place-exchange have been observed using atomic force microscopy during oxide formation on Cu(111) by Cruickshank and Gewirth[6]. The drawing of oxygen to the surface upon anodic charge was also observed in simulations by Koper and van Santen[52]. The change in metal-oxygen bond length for adsorbed O is greater than that noted for OH. This difference in potential sensitivity is due to the increased availability of oxygen electrons for interaction with the metal, and therefore a greater sensitivity to the Pauli repulsion effects. We compared the partial density of states (pDOS) for oxygen on Ni(111) in O *(ads)* and OH *(ads)* (Figure 9). The pDOS supports the above rationale, by showing oxygen *p* states that overlap completely with the Ni *d* band in the oxide, whereas OH maintains a non-interacting sigma OH bonding orbital resident below the Ni *d* band.

We find that the potential of zero charge for the doubly oxidized system moves 500 mV with respect to the unactivated water phase in the cathodic direction to -0.75 V NHE. A cathodic shift of the potential of zero charge implies that the Ni–O interaction creates a local enrichment of electrons on the metal surface. To maintain the same potential, therefore, electrons must be withdrawn from the system. In a potentiostatic sense, therefore, the formation of oxygen is electron releasing, whereas in the constant charge description, oxygen formation results in electron enrichment.

The net capacitance also changes from 9.0 $\mu F/cm^2$ (for H_2O) and 9.3 $\mu F/cm^2$ (for OH) to 11.2 $\mu F/cm^2$ (for O). This increase in capacitance is consistent with the shift in the potential of zero charge and indicates that the presence of O on the surface increases the

interfacial polarizability. This latter feature may be explained by the charge donation of oxygen to the surface, as discussed by Koper and van Santen[52].

The energies as a function of potential, E(V), for each surface configuration (all H_2O, H_2O+H, H_2O+OH and H_2O+O) are presented in Figure 10. From Figure 10 we can infer the potential dependence of the interfacial structure. The phase (*i.e.*, surface structure) with the most negative energy at any potential will be the dominant phase, according to the Boltzmann distribution.

There are several important features that may be distinguished from this phase diagram. First we observe the following ordering of stable phases, listed from cathodic to anodic: hydrogen overlayer up to -0.3 V NHE; at -0.5 V NHE, *before* hydrogen desorption (therefore there is a potential range over which both OH and H coexist on the surface), a hydroxyl overlayer is present; and for potentials above 0.2 V NHE the oxygen overlayer becomes preferred. These energies refer to 0 K *ab initio* results and are not corrected for zero point energies. These corrections will be applied in a later section. We include energetic terms such as the standard enthalpy of solvation of H^{+}[36] and hence are for systems exchanging with a strongly acidic bulk solution (pH 0). The interfacial chemistry at arbitrary pH will be considered in the subsequent section.

We find that the Ni(111)/$H_2O_{(aq)}$ interface is always activated regardless of potential, *i.e.*, there is no potential at which water by itself is the sole entity at the Ni(111)/H_2O interface. In this respect the current model is different from Cu(111)/$H_2O_{(aq)}$, for which there exists a potential window between -1.0V NHE and -0.5V NHE in which water is neither cathodically nor anodically activated on Cu(111), *i.e.*, the surface is inert. On Ni(111) we find that there is a region over which OH and H are predicted to coexist (-0.5

through to -0.3 V NHE). Competitive adsorption of OH and H on nickel surfaces has been noted in a kinetic study by Saraby-Reintjes[54].

Given the half-cell equilibrium potentials in Figure 10 we can deduce reactions that will be spontaneous at the Ni(111)/H_2O interface. For example, the reaction:

$$Ni(111) + OH^- + H^+ \rightarrow Ni(111)\text{-}H + Ni(111)\text{-}OH \quad [7]$$

has a potential difference of -0.8 V, based on the half-cell potentials of -0.3 V NHE and -0.5 V NHE for the reductive adsorption of hydrogen and the oxidative adsorption of OH^-, respectively. This is further evidence that H and OH will be coadsorbed on the Ni(111) surface in the absence of a specific polarization. The spontaneous dissociation of H_2O on Ni(111) was also predicted by Michaelides, Alavi and King[40] who showed that a partially dissociated bilayer of H_2O containing OH* and H* on Ni(111) was thermodynamically preferable to an intact water bilayer.

The subsequent reaction in which hydroxyl dissociates on the surface:

$$Ni(111)\text{-}OH \rightarrow Ni(111)\text{-}O + Ni(111)\text{-}H \quad [8]$$

has a smaller potential difference of -0.1 V, using the half-cell potentials of -0.3 V NHE for hydrogen adsorption and +0.2 V NHE for oxidative hydroxyl activation. We noted previously the correlation between enhanced oxygen adsorption and nickel dissolution (Figure 8). The spontaneous oxidation of H_2O and OH in concert with hydrogen adsorption therefore suggests a mechanism via which hydrogen activity at the surface can influence lattice oxidation and dissolution. Similar observations have been made by Saraby-Reintjes[54] and Song et al.[55]. The concurrence of such spontaneous chemistry also suggests that both mixed and high coverage surface phases must be explored to develop a greater understanding of interactions at the Ni(111)/H2O interface.

Surface chemistry at low, ambient and elevated temperatures

The intersection of energy functions in Figure 10 designates a phase transition, and the potential at which the transition occurs is the equilibrium or reversible potential for that transition. There is therefore a strong correspondence between the phase diagrams developed for *surfaces* in this study and the Pourbaix diagrams developed for solid-state transitions by Deltombe, de Zoubov, and Pourbaix[56] (a revised Pourbaix diagram for phase transitions of nickel has been constructed by Beverskog and Puigdomenech[57]). By calculating the relevant thermodynamic corrections to the 0 K energies presented in the previous section we have created analogous phase diagrams for chemistry occurring on the surface as a function of pH, potential and temperature.

Frequencies of vibration, zero point vibrational energies, and entropies have been calculated for the water, hydroxyl, oxide and hydrogen adsorbates bound at the Ni(111)|H_2O *(aq)* interface (Table 1). Frequencies were calculated using the harmonic approximation and by varying only the coordinates of the atoms comprising the adsorbed species. We tested the potential dependence of the vibrational corrections by calculating vibrational modes for adsorbed hydrogen at both the neutral (0.24 V) and a cathodic potential (-1.6 V), and found that both the zero point vibrational energy and the entropic terms differed by less that 0.01 kJ/mol. We therefore do not calculate the thermodynamic parameters at each potential, but assume that they are constant over the potential range. This assumption may break down for phases such as O that exhibit a greater variation in topology over a potential range.

The frequencies presented in Table 1 compare favorably with reported experimental values and results calculated in previous theoretical studies. While the librational and vibrational spectra of H_2O on Ni(111) has not hitherto been published, we find a high degree of similarity between our values and those observed on Pt(111)[58]. Similarly, our results for hydrogen compare favorably with the UHV high-resolution electron energy loss spectra of hydrogen adsorbed on Ni(111) by both Maynard et al.[59] (765, 110 cm^{-1}) and Yanagita et al.[60] (724, 925 and 1126 cm^{-1}). Nakamura's infra-red reflection absorption spectroscopy (IRAS) study of hydroxides on Ni(111) yielded a frequency of 930 cm^{-1}, not observed in this work, which they assigned to the formation of a bulk b-$Ni(OH)_2$ phase[21]. Currently there are no observations of the vibrational modes of oxygen on a Ni(111) surface, however, on Pt(111) a surface-stretching mode of 470 cm^{-1} was measured for oxygen by Parker, Bartram, and Koel[61].

Because water and hydroxyl activation require the exchange of protons with the surrounding environment, we must also include a free energy term for proton solvation. Following recent experimental and theoretical literature[36-39] we adopted a value of -1080 kJ/mol for proton solvation at 300 K and 1 M concentration, and subsequently derived a value of -970 kJ/mol for proton solvation at 600 K and 1 M concentration using high temperature parameters developed by Criss and Cobble[62-64]. Entropies of the reference H^+ *(g)* state at 1 atm were calculated using the Sackur-Tetrode equation.

Light species such as hydrogen are expected to readily diffuse across the surface at ambient and elevated temperatures. Using the barrier of 0.09 eV calculated in previous work, we use Hill's equation for the partition function of a particle in a model sinusoidal potential[65], and calculated additional entropies of diffusion to be 30.1 J/mol/K at 300 K

and 35.6 J/mol/K at 600 K. We neglected the calculation of entropies of diffusion for the heavier oxygen adsorbates.

The phase diagrams for inert and activated water phases on Ni(111) at 0, 300 and 600 K are presented in Figure 11. Differently shaded regions indicate the O, OH and H phases at 300 K, dashed lines represent phase transitions at 0 K and dotted lines represent phase transitions at 600 K. The phase diagram at absolute zero corresponds to the points extracted from Figure 10, with no pH dependence because the chemical potential of H^+ at absolute zero is constant. At 300 K and 600 K the phase transitions shift according to the chemical potential of H^+ by -0.06 and -0.12 V per pH unit, respectively. We remind the reader that there is some overlap between H and OH coverage of the Ni(111) surface and therefore the H/OH transition covers a range of 0.2 V.

Suzuki, Yamada and Itaya[20] studied the Ni(111) surface in contact with a Na_2SO_4/H_2SO_4 solution at pH 3 using scanning tunneling microscopy (STM) and found that the surface was bare and unreconstructed up to -0.16 V NHE (note: hydrogen is typically invisible to STM probes). Above this potential nickel begins to dissolve at the steps. At +0.09 V a surface film starts to form. While Suzuki et al. attribute this film to oxide formation, the in situ infrared spectroscopy and STM observations by Nakamura et al.[21] imply that the overlayer consists of hydroxyl species and ultimately $Ni(OH)_2$. Substantial surface reconstruction is observed as the nickel surface adopts the configuration of $Ni(OH)_2$. The hydroxyl transition point measured by Suzuki (pH 3, -0.16 V) lies within the potential region of surface coverage by hydroxyl calculated in this study, and the latter point for surface oxidation (pH 3, +0.09 V) lies within the region of oxygen coverage on the Ni(111) surface. The experimental transition points, therefore,

while coinciding with the appropriate regions of the phase diagram, do not fall upon the transition lines separating the phases. We suggest that this is because the present study has only considered phenomena occurring at low coverage. Models that include higher coverages and sufficient lateral interactions will be required to describe the formation of higher coverage overlayers as observed in the studies by Suzuki et al.[20] and Nakamura et al.[21].

We overlay the Pourbaix diagram for nickel calculated by Beverskog and Puigdomenech[57] upon the phase diagrams derived in this study in Figure 12 (a – 300 K, b – 600 K). At 300 K we note that the surface hydroxyl phase straddles the pure solid nickel phase, and edges over into the β-$Ni(OH)_2$ and $NiH_{0.5}$ phases. This indicates that hydroxyl is coadsorbed with hydrogen over some range, and that (when one sweeps anodically) the bulk β-$Ni(OH)_2$ phase will form before the hydroxide overlayer deprotonates to the oxide. At 600 K we see a similar overlap between surface and bulk regions. Here, however, the β-$Ni(OH)_2$ phase is not predicted from the Pourbaix diagram. Instead the NiO phase is dominant. We find here that the hydroxyl overlayer again forms on the (111) surface of pure solid Ni. In this case, however, as the potential is varied anodically we find that the formation of a surface oxide does occur before the formation of the next bulk phase, which happens to be the oxide. There is a much narrower range of potentials over which surface hydroxides can be observed. Moving towards cathodic potentials we predict an overlap region where hydroxides can form on the bulk nickel-hydride.

4. Summary

The ‘double reference’ method for studying electrochemical interfaces developed by Filhol and Neurock was applied to the study of water activation on a model Ni(111)/H_2O interface. Equilibrium potentials for the reductive adsorption of H^+ and the activation of water to OH and subsequently O were determined for both low and high temperature environments. The low-temperature equilibrium potentials for these reactions conform to qualitative expectations: hydrogen adsorbs at potentials cathodic of -0.3 V NHE, and competitively with hydroxyl adsorption over the range -0.5 to -0.3 V NHE. Hydroxide covers the surface between -0.3 V NHE and +0.2 V NHE, at which point the hydroxide species is deprotonated to form a surface oxide.

The discontinuities observed in stable phases at the interface are complemented by continuous changes occurring within the potential ranges of each phase. Water molecules rotate from hydrogen towards the surface at cathodic potentials, to a flat orientation at anodic potentials. The water is also drawn towards the surface upon anodic polarization. On the other hand, adsorbed hydrogen is repelled from, while both hydroxide and oxide are attracted to, the surface upon anodic polarization. We find that strengthening the metal-oxygen interaction by anodic surface polarization causes a simultaneous weakening of the surface Ni-Ni bonding, leading to the formation of a Ni adatom on the surface.

The computation of phase diagrams for water and its dissociation products on a Ni(111) substrate at ambient and elevated temperatures was also performed. The modeling of vibrational, diffusional and translational degrees of freedom allows a multi-dimensional description of the electrochemical surface chemistry in terms of potential, temperature and pH. The phase diagram mapped out at 300 K is in agreement with the

limited experimental data that are available for this surface, and good agreement is seen with the solid-state phase diagrams developed by Pourbaix. The presence of surface hydroxyl species is quantitatively predicted to be the natural precursor to the buildup of the β-$Ni(OH)_2$ phase, and, at 600 K, the precursor to surface oxygen overlayers which later generate the bulk oxide. The natural development of this work to higher coverage adsorption systems should lead to a greater understanding of the formation of the bulk hydroxide and oxide phases represented in these diagrams.

Although the results presented in this paper offer an important degree of insight into the processes affecting both substrate and solvent species at the electrochemical Ni/H_2O interface, they are limited by the fact that only a single sampling of the surrounding solvent structure was used. In reality many such structures are being sampled with turnover frequencies of the order of picoseconds. We envisage that ensembles of such systems can be sampled in the near future using *ab initio* molecular dynamics. In this way ensemble averaged phase diagrams can be produced. The development of improved electrolyte models is also of great importance, perhaps using similar strategies to those developed by Spohr[66] and Dimitrov[67].

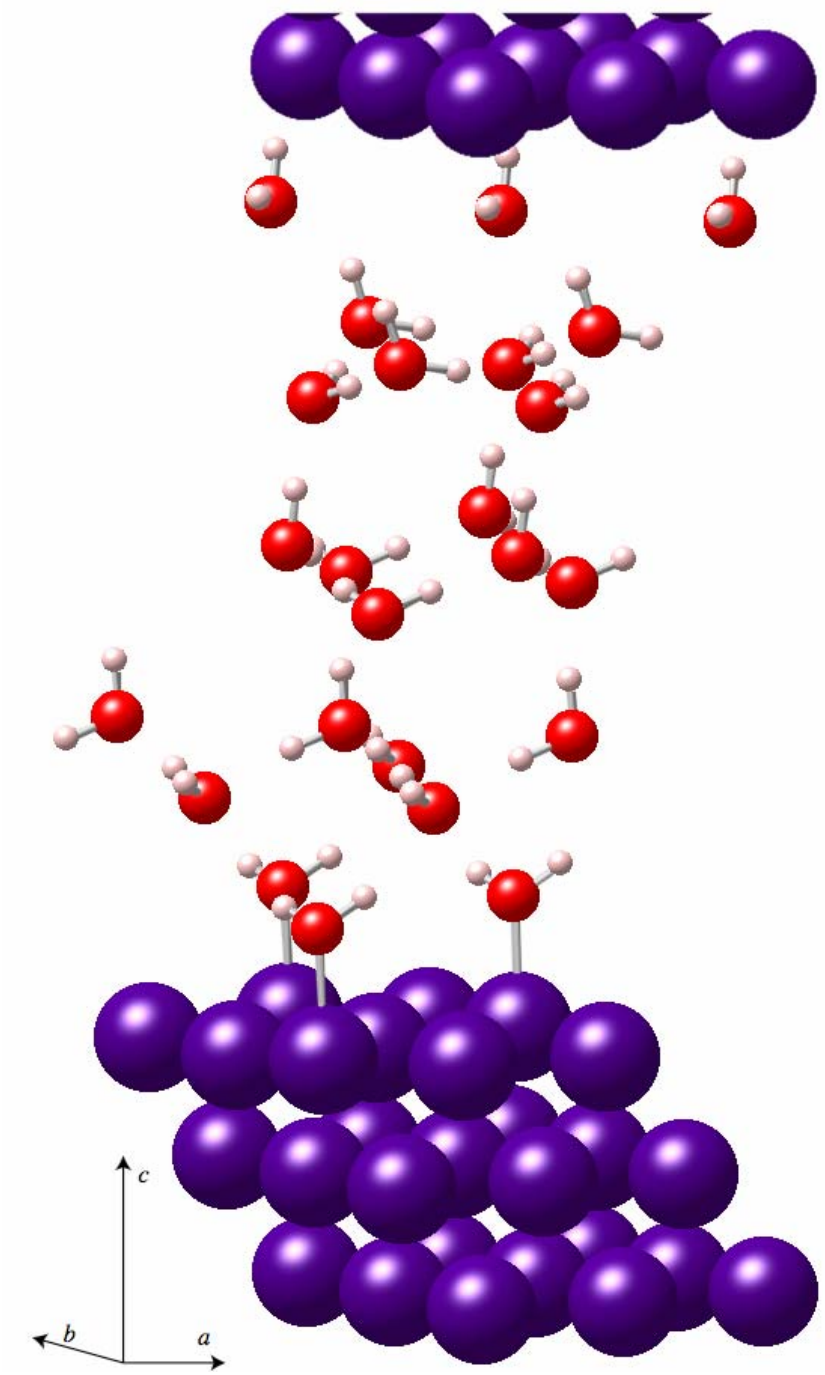

Figure 1. The periodic supercell (which extends in all three dimensions) containing 24 water molecules arranged in a multiple bilayer network, and 27 nickel atoms arranged into three (111) close packed planes.

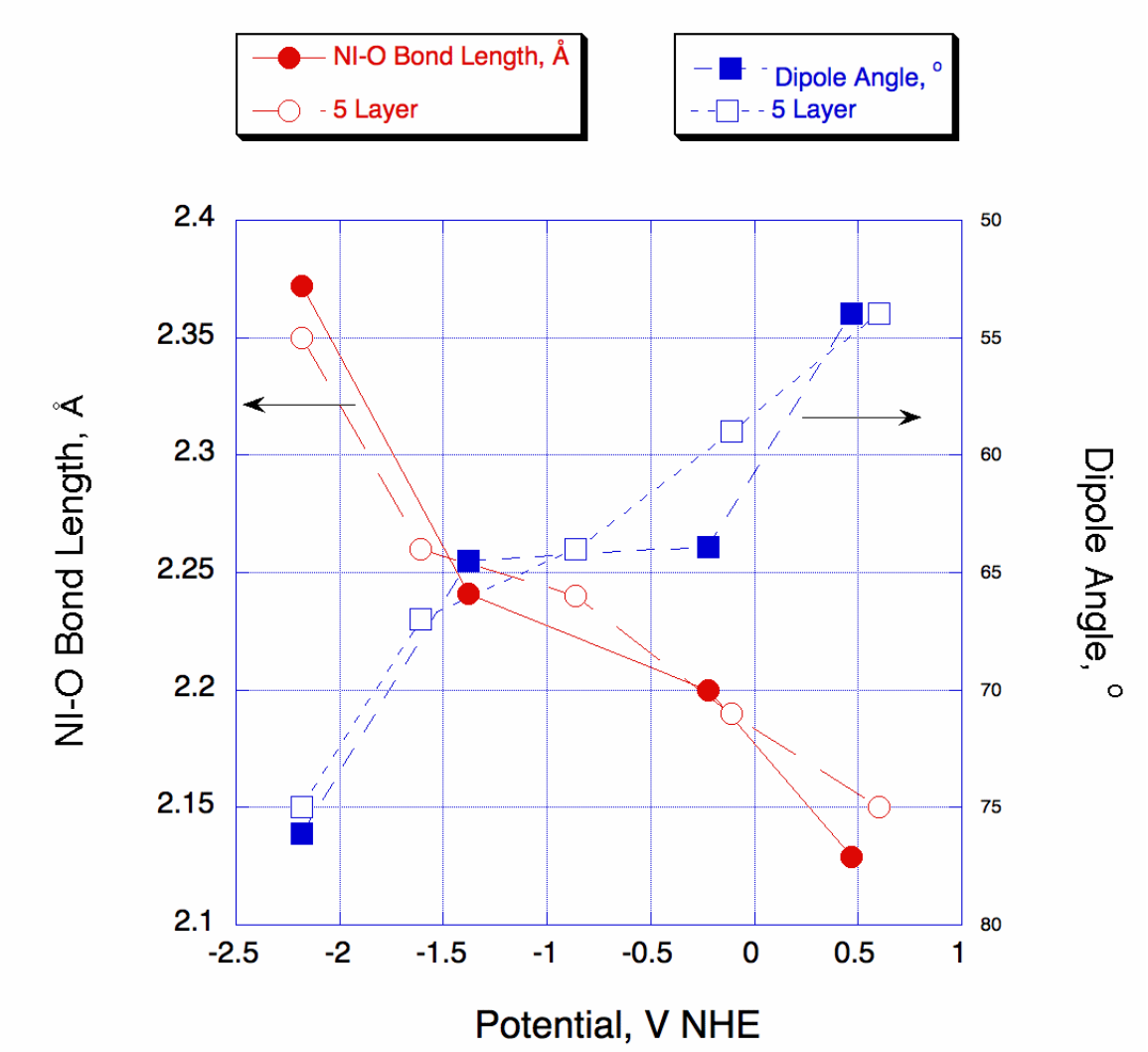

Figure 2. Water dipole orientation, given as the declination of the water dipole from the surface normal, and the water distance from the electrode presented as a function of potential. Results are shown for two slab thicknesses: three layers of Ni(111) planes (filled symbols), and five layers of Ni(111) planes (open symbols).

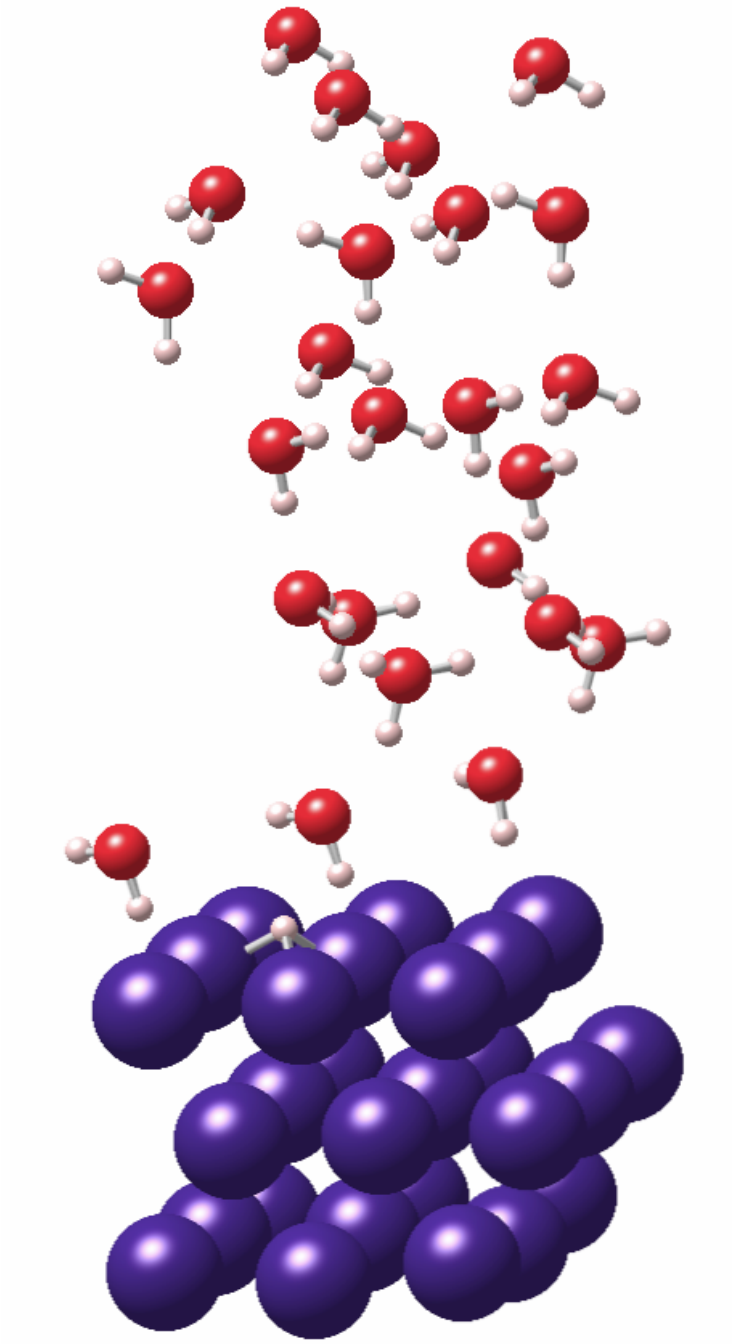

Figure 3. Ni-H supercell. H adsorbs in the hcp hollow site, beneath the cathodically oriented (H-down) water monolayer.

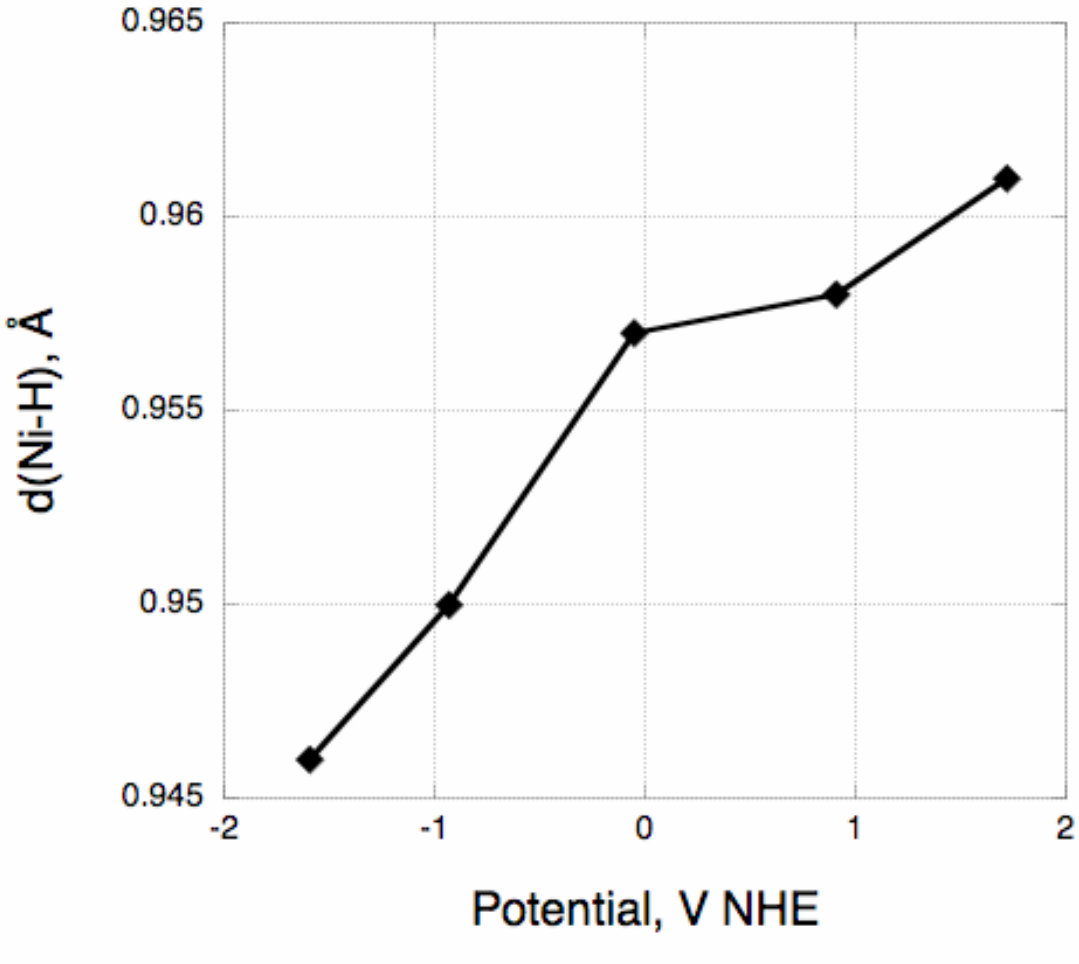

Figure 4. Variation in the Ni(111) surface - hydrogen distance (the height of hydrogen above the surface plane) at the hcp site as a function of electrochemical potential.

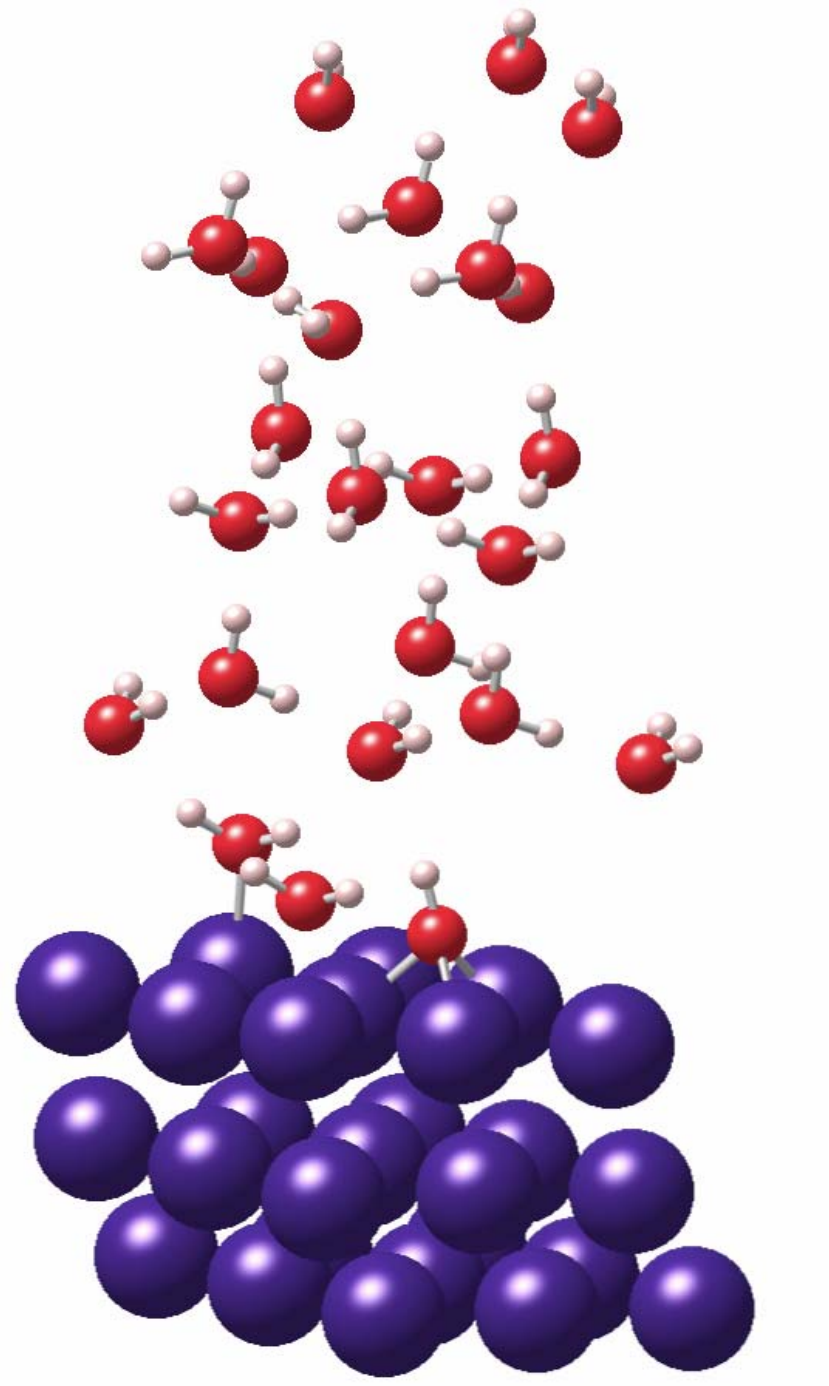

Figure 5. The Ni(111)-OH supercell. The hydroxyl species adsorbs at the three fold hollow, and maintains some hydrogen bonding interactions with the surrounding water network. The hydroxyl oxygen sits 1.66 Å above the surface plane.

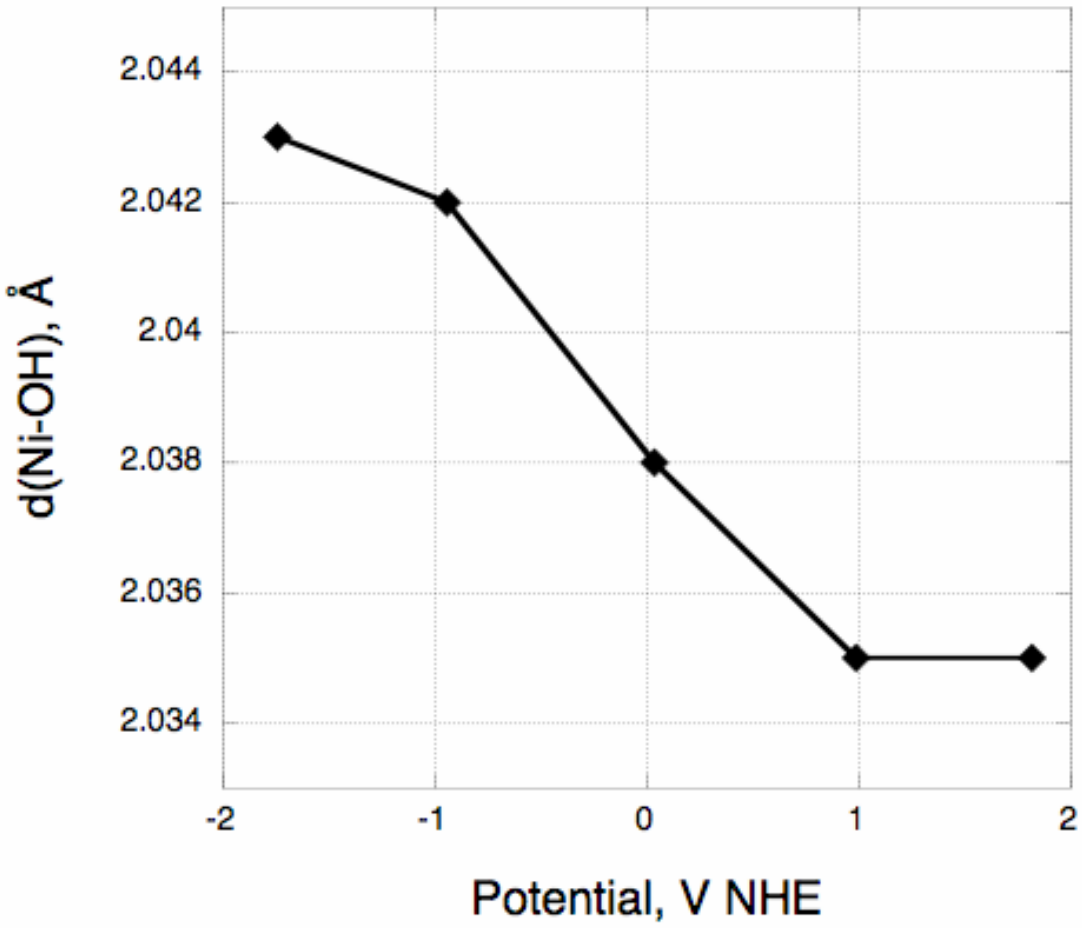

Figure 6. Variation in the Ni(111) surface - oxygen distance for adsorbed hydroxyl (the height of the oxygen atom above the surface plane) at the hcp site as a function of electrochemical potential.

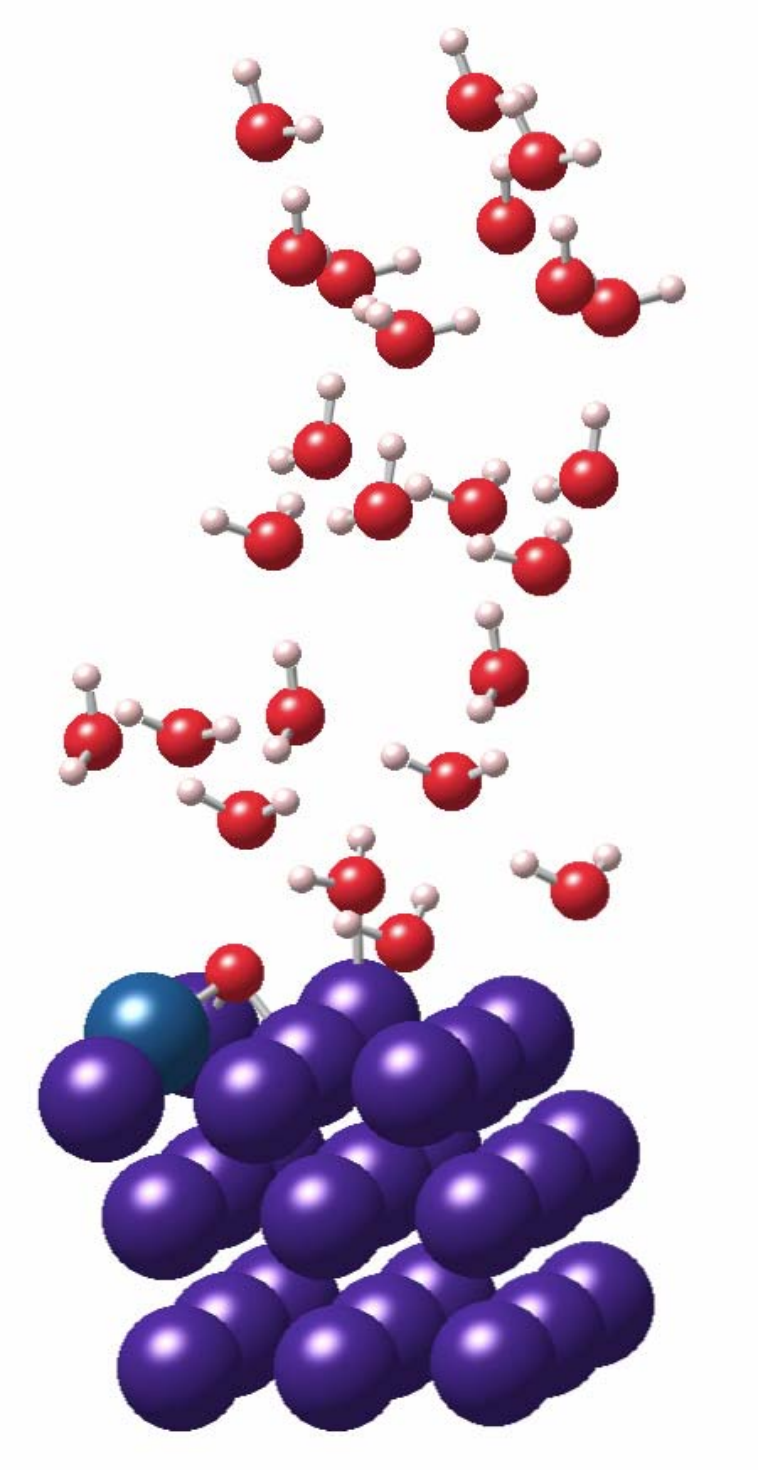

Figure 7. The Ni(111)-O supercell. The oxygen atom sits in a three hold hollow site, and has minimal interaction with the surrounding water matrix. Note that one of the nickel atoms connected to oxygen is slightly raised above the surface plane at the potential of zero charge.

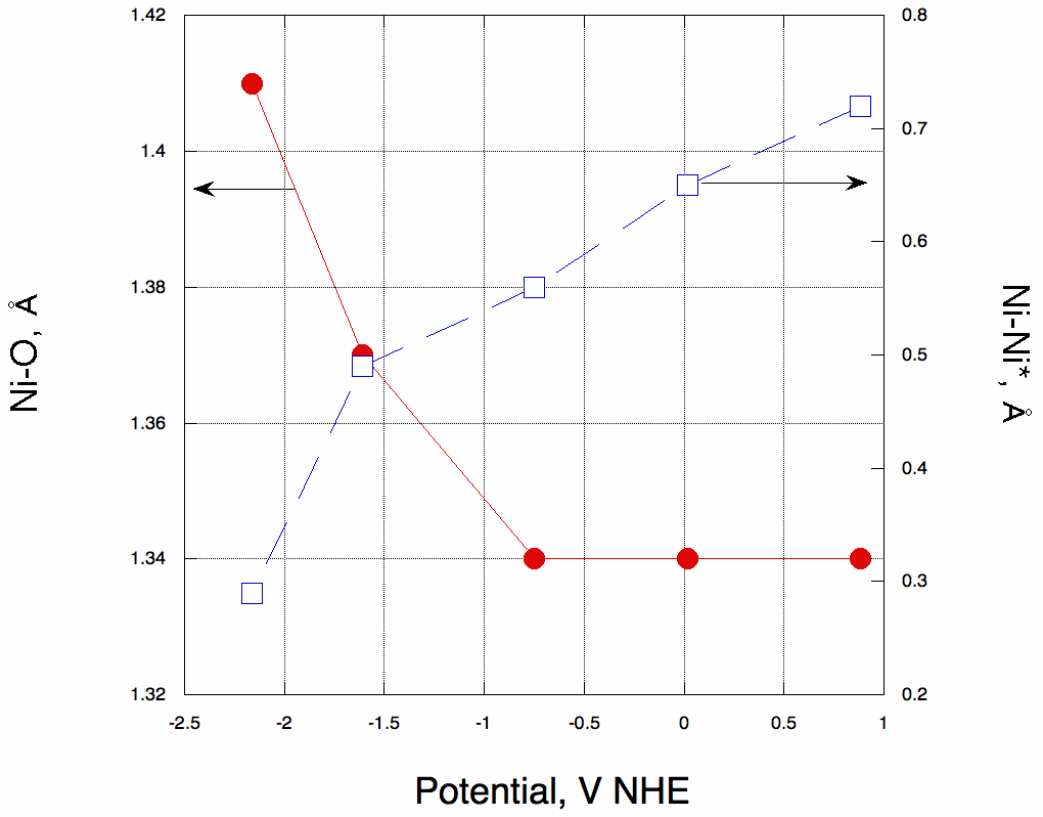

Figure 8. The heights of adsorbed atomic oxygen (circles) and a perturbed nickel atom (squares) above the surface (111) plane as a function of electrochemical potential for the Ni(111)-O/$H_2O_{(aq)}$ interface.

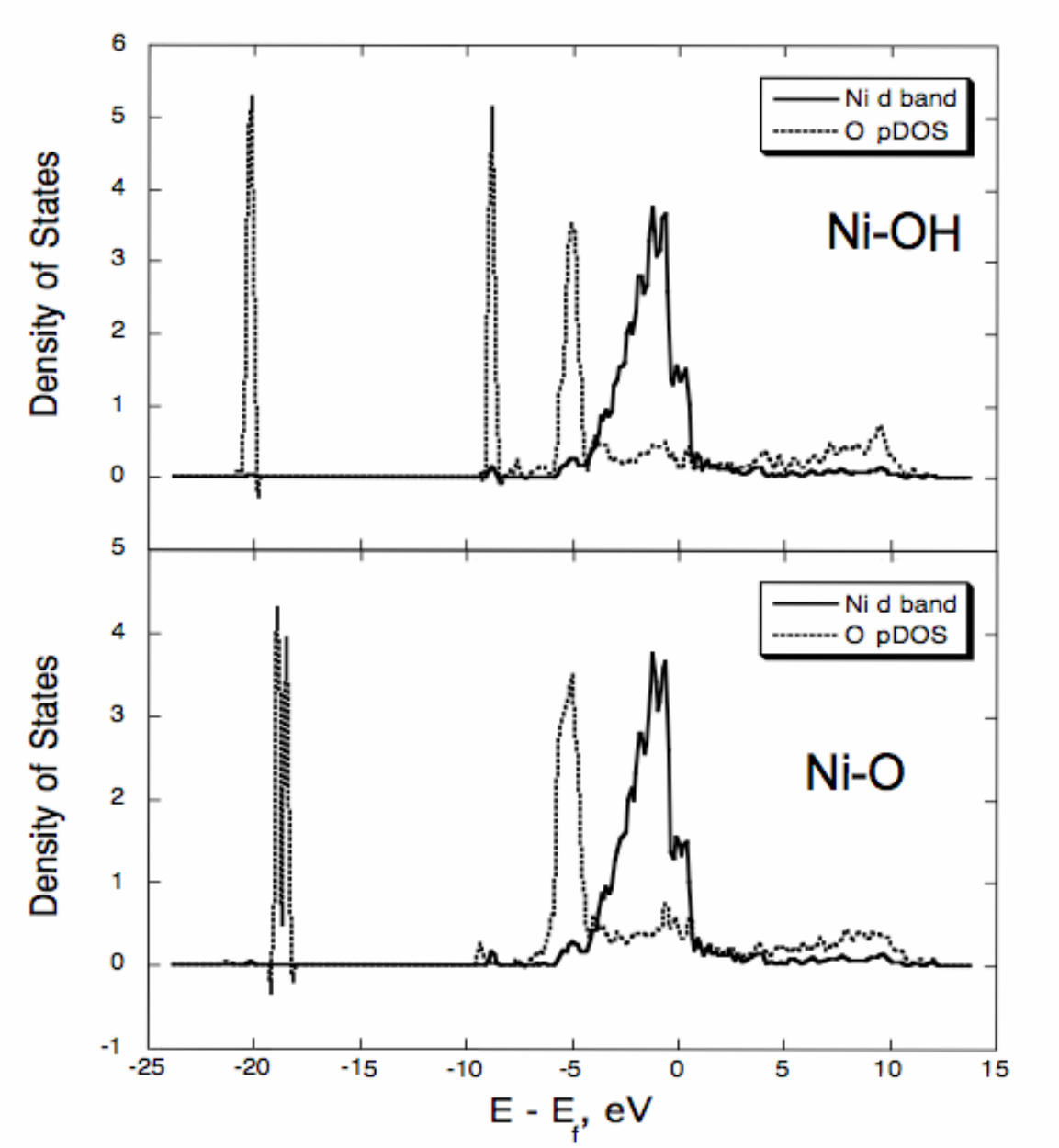

Figure 9. Partial density of states for the Nickel d-band (solid line) and for the oxygen atom of OH (top – dashed line) and O (bottom – dashed line).

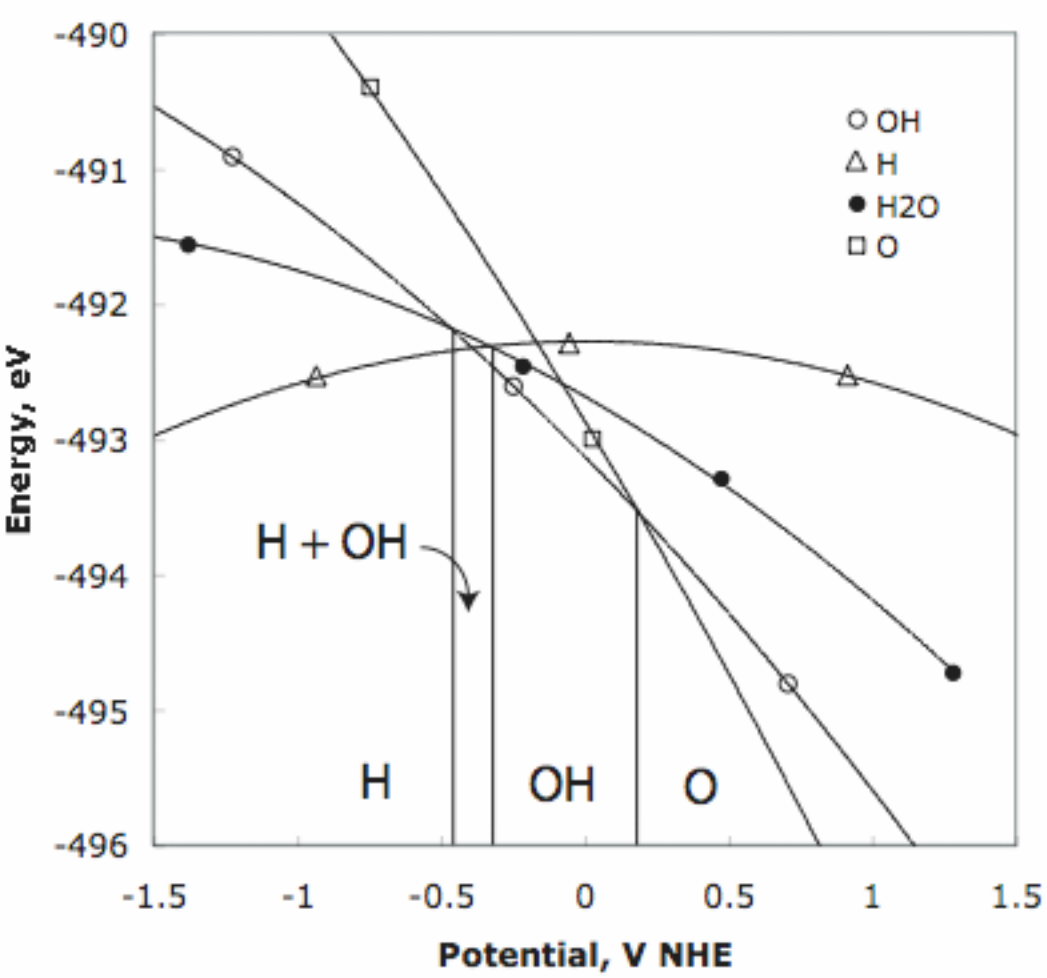

Figure 10. Phase diagram for surface hydride, molecular water, hydroxy and oxy species on Ni(111).

Table 1. Vibrational frequencies, zero point energies and entropic contributions calculated for water, hydrogen, hydroxyl and oxygen adsorbed on the Ni(111)/H_2O interface. Contributions due to coupling with Ni and H_2O environment were not explicitly determined.

	Frequency, cm^{-1}	ZPVE, kJ/mol	TS (300 K), kJ/mol	TS (600 K), kJ/mol
H_2O	190, 271, 386, 586, 905, 1100, 1283, 3503, 3673	71.2	7.00	29.8
H (hcp)[a]	797, 841, 1151	16.7	0.56	5.96
H (hcp)[b]	810, 838, 1141	16.7	0.55	5.95
OH	208, 261, 418, 681, 711, 3552	24.9	6.63	27.1
O	350, 371, 478	7.18	3.74	16.3

[a.] Vibrational calculation performed under neutral simulation cell conditions (V = -0.3 V NHE).

[b.] Vibrational calculation performed under cathodic cell conditions (V = -1.6 V NHE)

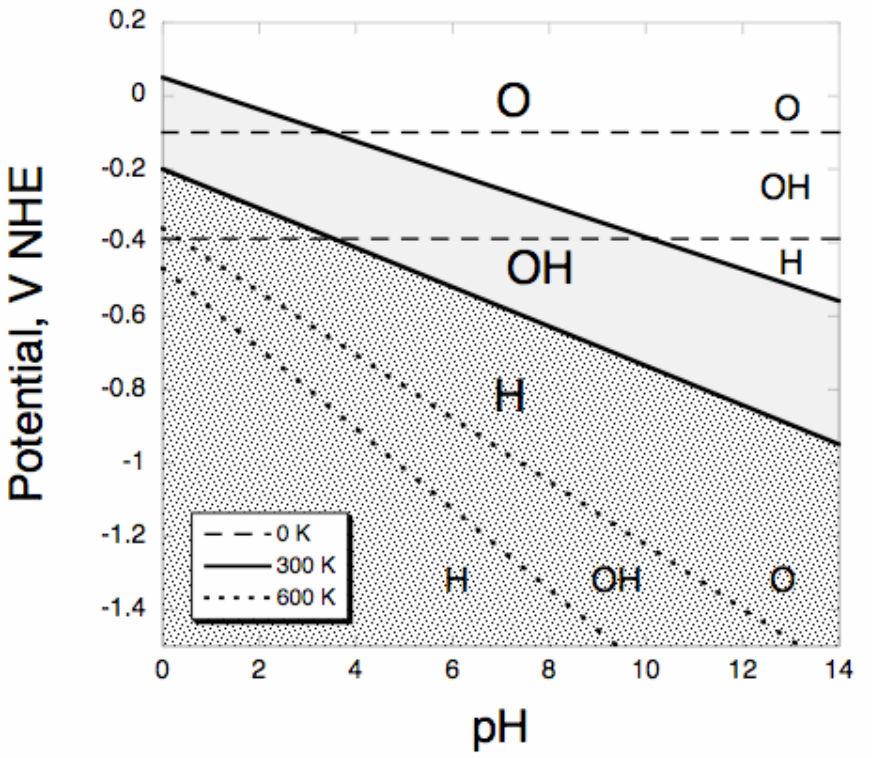

Figure 11. Potential-pH phase diagram for the dissociated states of water at the Ni(111)/H_2O interface at 0 K, 300 K, and 600 K.

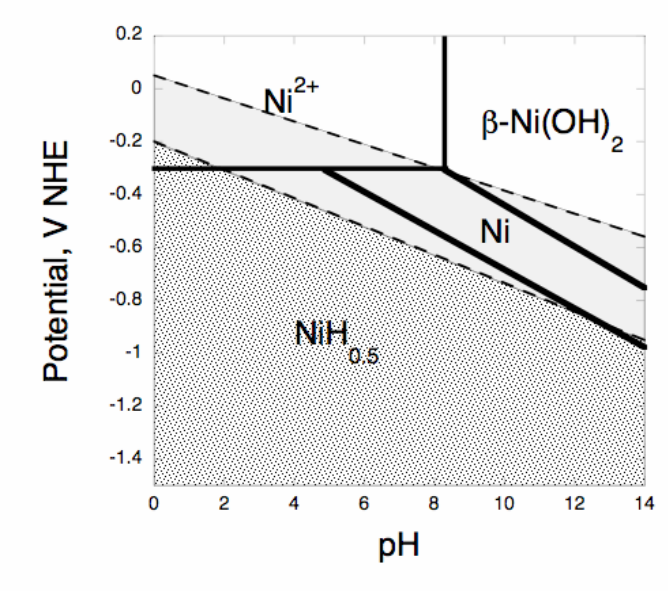

(a)

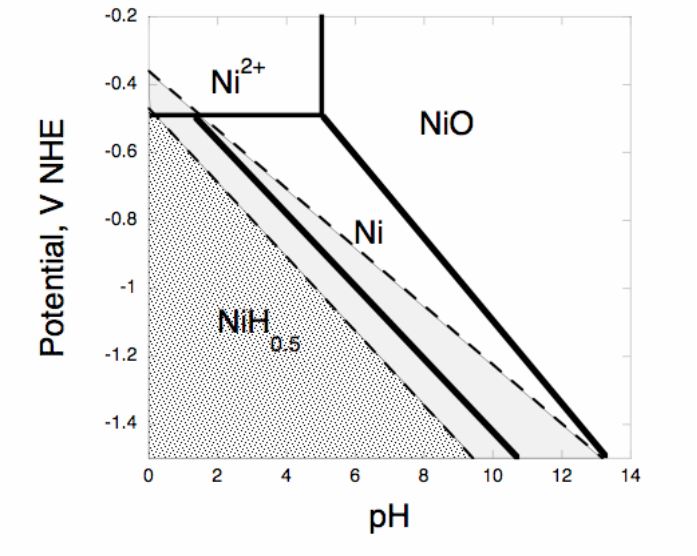

(b)

Figure 12. *Ab initio* derived surface phase diagrams and surface phase diagrams (dashed lines with shaded regions – white O, pale gray OH, dark gray H) plotted together with the experimental Pourbaix diagrams (overlaid on top with bold lines) at (a) 300 K and (b) 600 K.

5. References

(1) Kolb, D. M., *Angew. Chem. Int. Ed. Engl.* **2001,** *40*, 1162-1181.
(2) Kolb, D. M.; Kibler, L. A., *Zeit. Phys. Chem.* **2003,** *217*, 1265-1280.
(3) Bewick, A.; Kunimatsu, K., *Surf. Sci.* **1980,** *101*, 131-138.
(4) Iwasita, T.; Nart, F. C., *Prog. Surf. Sci.* **1997,** *55*, 271-340.
(5) Kunze, J.; Maurice, V.; Klein, L. H.; Strehblow, H.-H.; Marcus, P., *Corrosion Sci.* **2004,** *46*, 245-264.
(6) Cruickshank, B. J.; Sneddon, D. D.; Gewirth, A. A., *Surf. Sci. Lett.* **1993,** *281*, 308-314.
(7) Niaura, G., *Electrochim. Acta* **2000,** *45*, 3507-3519.
(8) Wilms, M.; Broekmann, P.; Stuhlmann, C.; Wandelt, K., *Surf. Sci.* **1998,** *416*, 121-140.
(9) Bockris, J. O. M.; Jeng, K. T., *Adv. Colloid. Interface. Sci.* **1990,** *33*, 1-54.
(10) Anderson, A. B., *Electrochim. Acta* **2003,** *48*, 3743-3749.
(11) Sidik, R. A.; Anderson, A. B., *J. Electroanal. Chem* **2002,** *528*, 69-76.
(12) Trasatti, S., *Electrochim. Acta* **1991,** *36*, 1659-1667.
(13) Crispin, X.; Geskin, V. M.; Bureau, C.; Lazzaroni, R.; Schmickler, W.; Bredas, J. L., *J. Chem. Phys.* **2001,** *115*, 10493-10499.
(14) Michaelides, A.; Ranea, V. A.; de Andres, P. L.; King, D. A., *Phys. Rev. Lett.* **2003,** *90*, 216102-216106.
(15) Filhol, J.-S.; Neurock, M., *(unpublished)*.
(16) Chapman, D. L., *Phil. Mag.* **1913,** *25*, 475.
(17) Guoy, G., *J. Phys.* **1910,** *9*, 457.
(18) Taylor, C. D.; Wasileksi, S. A.; Fanjoy, J. W.; Filhol, J.-S.; Neurock, M., *Phys. Rev. B. (submitted)* **2005**.
(19) Attanasio, S. A.; Morton, D. S. In *Measurement of the Nickel/Nickel Oxide Transition in Ni-Cr-Fe Alloys and Updated Data and Correlations to Quantify the Effet of Aqueous Hydrogen on Primary Water SCC*, 11th Intl. Conference on Environmental Degradation of Materials in Nuclear Systems, Stevenson, WA, 2003; Stevenson, WA, 2003.
(20) Suzuki, T.; Yamada, T.; Itaya, K., *J. Phys. Chem.* **1996,** *100*, 8954-8961.
(21) Nakamura, M.; Ikemiya, N.; Iwasaki, A.; Suzuki, Y.; Ito, M., *J. Electroanal. Chem* **2004,** *566*, 385-391.
(22) Maurice, V.; Strehblow, H.-H.; Marcus, P., *Surf. Sci.* **2000,** *458*, 185-194.
(23) Kunze, J.; Maurice, V.; Klein, L. H.; Strehblow, H.-H.; Marcus, P., *Electrochim. Acta* **2003,** *48*, 1157-1167.
(24) Kunze, J.; Maurice, V.; Klein, L. H.; Strehblow, H.-H.; Marcus, P., *J. Phys. Chem. B.* **2001,** *105*, 4263-4269.
(25) Strehblow, H.-H.; Maurice, V.; Marcus, P., *Electrochim. Acta* **2001,** *46*, 3755-3766.
(26) Taylor, C. D.; Kelly, R. G.; Neurock, M., *J. Electrochem. Solid State Lett. (submitted)* **2005**.
(27) Kresse, G.; Furthmuller, J., *Phys. Rev. B.* **1996,** *54*, 11169-11186.
(28) Kresse, G.; Furthmuller, J., *Comput. Mater. Sci.* **1996,** *6*, 15-50.

(29) Kresse, G.; Hafner, J., *Phys. Rev. B.* **1993,** *47*, 558-561.
(30) Vanderbilt, D., *Phys. Rev. B.* **1990,** *41*, 7892-7895.
(31) Kresse, G.; Hafner, J., *J. Phys.: Condens. Matter* **1994,** *6*, 8245.
(32) Perdew, J. P.; Burke, K.; Ernzerhof, M., *Phys. Rev. Lett.* **1996,** *77*, 3865.
(33) Perdew, J. P.; Burke, K.; Ernzerhof, M., *Phys. Rev. Lett.* **1998,** *80*, 891.
(34) Monkhorst, H. J.; Pack, J. D., *Phys. Rev. B.* **1976,** *13*, 5188-5192.
(35) Llano, K.; Eriksson, L. A., *J. Chem. Phys.* **2002,** *117*, 10193-10206.
(36) Mejias, J. A.; Lago, S., *J. Chem. Phys.* **2000,** *113*, 7306-7316.
(37) Tissandier, M. D.; Cowen, K. A.; Feng, W. Y.; Gundlach, E.; Cohen, M. H.; Earhart, A. D.; Coe, J. V.; Tuttle Jr., T. R., *J. Phys. Chem. A.* **1998,** *102*, 7787-7794.
(38) Hummer, G.; Pratt, L. R.; Garcia, A. E., *J. Phys. Chem.* **1996,** *100*, 1206-1215.
(39) Magnera, T. F.; David, D. E.; Michl, J., *Chem. Phys. Lett.* **1991,** *182*, 363-370.
(40) Michaelides, A.; Alavi, A.; King, D. A., *Phys. Rev. B.* **2004,** *69*, 113404-113407.
(41) Nakamura, M.; Ito, M., *Chem. Phys. Lett.* **2004,** *384*, 256-261.
(42) Sebastiani, D.; Delle Site, L., *J. Chem. Theory Comput.* **2005,** *1*, 78-82.
(43) Price, D. L.; Halley, J. W., *J. Chem. Phys.* **1995,** *102*, 6603-6612.
(44) Iedema, M. J.; Dresser, M. J.; Doering, D. L.; Rowland, J. B.; Hess, W. P.; Tsekouras, A. A.; Cowin, J. P., *J. Phys. Chem. B.* **1998,** *102*, 9203-9214.
(45) Nield, V. M.; Whitworth, R. W., *J. Phys.: Condens. Matter* **1995,** *7*, 8259-8271.
(46) Baer, R.; Zeiri, Y.; Kosloff, R., *Phys. Rev. B.* **1997,** *55*, 10952-10974.
(47) Greeley, J.; Mavrikakis, M., *Surf. Sci.* **2003,** *540*, 215-229.
(48) Taylor, C. D., *J. Electrochem. Soc.* **2005**.
(49) Watson, G. W.; Wells, R. P. K.; Willock, D. J.; Hutchings, G. J., *J. Phys. Chem. B.* **2000,** *104*, 6439-6446.
(50) The pH of the model system is uncalculable since the finite number of protons and hydroxyl species in the water matrix is zero.
(51) Patrito, E. M.; Paredes-Olivera, P., *Surf. Sci.* **2003,** *527*, 149-162.
(52) Koper, M. T. M.; van Santen, R. A., *J. Electroanal. Chem* **1999,** *472*, 126-136.
(53) Taylor, C. D.; Kelly, R. G.; Neurock, M., *(unpublished)*.
(54) Saraby-Reintjes, A., *Electrochim. Acta* **1985,** *30*, 387-401.
(55) Song, K.-D.; Kim, K. B.; Han, S.; Lee, H. K., *Electrochemistry Communications* **2003,** *5*, 460-466.
(56) Deltombe, E.; de Zoubov, N.; Pourbaix, M., *Atlas of Electrochemical Equilibria in Aqueous Solution*. ed.; NACE: Houston, Texas, 1974.
(57) Beverskog, B.; Puigdomenech, I., *Corr. Sci.* **1997,** *39*, 969-980.
(58) Jacobi, K.; Bedurftig, K.; Wang, Y.; Ertl, G., *Surf. Sci.* **2001,** *472*, 9-20.
(59) Maynard, K. J.; Johnson, A. D.; Daley, S. P.; Ceyer, S. T., *Faraday Discuss.* **1991,** *91*, 437-449.
(60) Yanagita, H.; Sakai, J.; Aruga, T.; Takagi, N.; Nishijima, M., *Phys. Rev. B.* **1997,** *56*, 14952-14955.
(61) Parker, D. H.; Bartram, M. E.; Koel, B. E., *Surf. Sci.* **1989,** *217*, 489-510.
(62) Cobble, J. W., *J. Am. Chem. Soc.* **1964,** *86*.
(63) Cobble, J. W., *J. Am. Chem. Soc.* **1964,** *86*, 5390-5393.
(64) Criss, C. M.; Cobble, J. W., *J. Am. Chem. Soc.* **1964,** *86*, 5385-5390.
(65) Masel, R. I., *Principles of adsorption and reaction of solid surfaces*. ed.; Wiley Interscience: 1996.

(66) Spohr, E., *Solid State Ionics* **2002,** *150*, 1-12.
(67) Dimitrov, D. I.; Raev, N. D., *J. Electroanal. Chem.* **2000,** *486*, 1-8.